Gravitational wave signals of pseudo-Goldstone dark matter in the $\mathbb{Z}_3$ complex singlet model

Kristjan Kannike,[*] Kaius Loos,[†] and Martti Raidal[‡]

National Institute of Chemical Physics and Biophysics, Rävala 10, Tallinn 10143, Estonia

(Received 7 August 2019; accepted 14 January 2020; published 3 February 2020)

We study pseudo-Goldstone dark matter in the $\mathbb{Z}_3$ complex scalar singlet model. Because the direct detection spin-independent cross section is suppressed, such dark matter is allowed in a large mass range. Unlike in the original model stabilized by a parity and due to the cubic coupling of the singlet, the $\mathbb{Z}_3$ model can accommodate first-order phase transitions that give rise to a stochastic gravitational wave signal potentially observable in future space-based detectors.

DOI: 10.1103/PhysRevD.101.035001

I. INTRODUCTION

One of the best candidates for the dark matter (DM) is a scalar singlet [1,2]. The properties of singlet DM have been studied in detail [3–6] (see [7,8] for recent reviews; see also Refs. therein). The nonobservation of dark matter by direct detection experiments [9–11], however, puts severe bounds on models of DM comprised of weakly interacting massive particles (WIMP), pushing the mass of the singlet scalar DM—except around the Higgs resonance—over 1 TeV.

A way to suppress the direct detection cross section is to consider as the DM candidate a pseudo-Goldstone with derivative couplings to CP-even states [12] (the DM phenomenology of the imaginary part of the complex scalar singlet was first considered in [3,13], but only in the Higgs resonance region). Because the velocity of DM particles in the Galaxy is small, the prospective signal is suppressed by vanishing momentum transfer. This result remains practically unaffected when loop corrections to the direct detection cross section are taken into account [14,15]. Despite that, it is possible for pseudo-Goldstone DM to show up at the LHC [16–19]. Pseudo-Goldstone DM with two Higgs doublets was considered in [20].

In this class of models, the global $U(1)$ symmetry is explicitly, but only softly, broken into a discrete subgroup which is then broken spontaneously. In Ref. [12], the $U(1)$ group was explicitly broken into $\mathbb{Z}_2$ symmetry. We study the consequences of breaking $U(1)$ into $\mathbb{Z}_3$. The model admits two phases that produce a dark matter candidate. Firstly, the unbroken $\mathbb{Z}_3$ symmetry stabilizes S as a dark matter candidate. Secondly, with the broken $\mathbb{Z}_3$ symmetry, the imaginary part of S, denoted by χ, is still stable due to the $S \to S^\dagger$ symmetry of the Lagrangian. The main difference between the $\mathbb{Z}_2$ and $\mathbb{Z}_3$ pseudo-Goldstone DM models is that the potential of the latter contains a cubic S^3 term. There are other possible cubic terms [21–23], but they do not respect the $\mathbb{Z}_3$ symmetry.

To this date, the $\mathbb{Z}_3$-symmetric complex singlet model has been studied in the unbroken phase. Originally, the model was proposed in the context of neutrino physics [24]. Detailed analysis of DM phenomenology was carried out in Ref. [25]. Indirect detection of $\mathbb{Z}_3$ DM was considered in [26,27]. The cubic coupling can contribute to $3 \to 2$ scattering for $\mathbb{Z}_3$ strongly interacting (SIMP) DM [28–31]. The effects of early kinetic decoupling were studied in [32]. The $\mathbb{Z}_3$ symmetry has been considered as the remnant of a dark $U(1)$ local [33–35] or global [36] symmetry. In the unbroken phase, the direct detection cross section can also be suppressed if the DM relic density is determined by semiannihilation processes [37–42]. However, the suppression is not as large as for pseudo-Goldstone DM.

The discovery of gravitational waves (GWs) by the LIGO experiment [43,44] opened a new avenue to probe new physics. First-order phase transitions generate a stochastic GW background [45–47], which may be discoverable in future space-based GW interferometers [48,49]. While the SM Higgs phase transition is a smooth crossover [50,51] and does not generate a GW signal, in models with an extended scalar sector, the first-order phase transition in the early Universe can become testable by observations. For a recent review on phase transitions and GWs, see Ref. [52].

GWs from beyond-the-SM physics with a scalar singlet have been studied in detail. These models admit a two-step phase transition that can be of the first order [53–60] and

[*]kristjan.kannike@cern.ch
[†]kaius.loos@gmail.com
[‡]martti.raidal@cern.ch

can potentially produce a measurable GW signal [61–72]. However, in the $\mathbb{Z}_2$ pseudo-Goldstone model, all phase transitions leading to the correct vacuum are of the second order [73], yielding no stochastic GW signal and excluding the additional potentially powerful experimental test of this class of the SM models. The phenomenology of phase transitions and GWs of the $\mathbb{Z}_3$ complex singlet model was studied in detail in Ref. [74] for the case where only the Higgs boson has a VEV in our vacuum. This work, however, disregarded the singlet as a DM candidate, because in the unbroken phase, a sizeable GW signal is incompatible with the correct relic density.

The goal of this paper is to study the nature of phase transitions and GW signals in the complex scalar singlet model in which a $U(1)$ symmetry is softly broken into its $\mathbb{Z}_3$ subgroup. Just like in the $\mathbb{Z}_2$ case, the elastic scattering cross section pseudo-Goldstone DM with matter can be small enough for the DM to be well hidden from direct detection. We find, however, that unlike in the $\mathbb{Z}_2$ case, strong first-order phase transitions can take place because the potential contains a cubic term. The resulting stochastic GW background is potentially discoverable in future space-based detectors such as LISA and BBO.

The paper is organized as follows. We introduce the model in Sec. II. Various theoretical and experimental constraints are discussed in Sec. III. DM relic density, phase transitions, and the predictions for the direct detection and GW signals are treated in Sec. IV. We conclude in Sec. V. The details on the effective potential and thermal corrections are relegated to the Appendix.

II. $\mathbb{Z}_3$ COMPLEX SINGLET MODEL

The most general renormalizable scalar potential of the Higgs doublet H and the complex singlet S, invariant under the $\mathbb{Z}_3$ transformation $H \to H$, $S \to e^{i2\pi/3}S$, is given by

$$V = \mu_H^2|H|^2 + \lambda_H|H|^4 + \mu_S^2|S|^2 + \lambda_S|S|^4 + \lambda_{SH}|S|^2|H|^2 + \frac{\mu_3}{2}(S^3 + S^{\dagger 3}), \tag{1}$$

where only the cubic μ_3 term softly breaks a global $U(1)$ symmetry. Notice that the $\mathbb{Z}_3$ symmetry precludes any quartic couplings that would result in a *hard* breaking of the $U(1)$. The potential Eq. (1)—just like in the original $\mathbb{Z}_2$ pseudo-Goldstone DM model—has an additional discrete $\mathbb{Z}_2$ symmetry, $S \to S^\dagger$.

In the unitary gauge, we parametrize the fields as

$$H = \begin{pmatrix} 0 \\ \frac{v+h}{\sqrt{2}} \end{pmatrix}, \qquad S = \frac{v_s + s + i\chi}{2}. \tag{2}$$

The $S \to S^\dagger$ is then equivalent to $\chi \to -\chi$, which makes χ stable even as the $\mathbb{Z}_3$ symmetry is broken. The model thus admits two different DM candidates: in the unbroken $\mathbb{Z}_3$ phase, the complex singlet S is a DM candidate, while in the broken $\mathbb{Z}_3$ phase, it is its imaginary part, the pseudo-Goldstone χ, which can be the DM. We concentrate on the latter case. (In order to avoid domain walls [75–79] due to the broken $\mathbb{Z}_3$, we can add to the potential a small term that explicitly breaks $\mathbb{Z}_3$, such as the linear term in S, but otherwise does not change the dark matter phenomenology.)

Without a loss of generality, the vacuum expectation value (VEV) of S can be taken to be real and positive, because the degenerate vacua, where χ has a nonzero VEV, are related to the real vacuum by $\mathbb{Z}_3$ transitions. This choice corresponds to a negative value of the parameter μ_3.

The stationary point conditions are

$$h(2\lambda_H h^2 + 2\mu_H^2 + \lambda_{SH}s^2) = 0, \tag{3}$$

$$s(4\lambda_S s^2 + 3\sqrt{2}\mu_3 s + 4\mu_S^2 + 2\lambda_{SH}h^2) = 0. \tag{4}$$

We see that the model admits four types of extrema: the origin as $\mathcal{O} \equiv (0,0)$ is fully symmetric; the vacuum $\mathcal{H} \equiv (v_h, 0)$, with Higgs VEV only, spontaneously breaks the electroweak symmetry; the vacuum $\mathcal{S} \equiv (0, v_s)$, with S VEV only, spontaneously breaks $\mathbb{Z}_3$; our vacuum $\mathcal{HS} \equiv (v_h, v_s)$ breaks both symmetries.

The mass matrix of CP-even scalars in our $\mathcal{HS}$ vacuum is given by

$$M^2 = \begin{pmatrix} 2\lambda_H v^2 & \lambda_{SH} v v_s \\ \lambda_{SH} v v_s & 2\lambda_S v_s^2 + \frac{3}{2\sqrt{2}}\mu_3 v_s \end{pmatrix}. \tag{5}$$

The mass matrix (5) is diagonalized by an orthogonal matrix,

$$O = \begin{pmatrix} \cos\theta & -\sin\theta \\ \sin\theta & \cos\theta \end{pmatrix}, \tag{6}$$

via $\mathrm{diag}(m_1^2, m_2^2) = O^T M^2 O$. The mixing angle θ is given by

$$\tan 2\theta = \frac{\lambda_{SH} v v_s}{\lambda_H v^2 + \lambda_S v_s^2 - \frac{3}{4\sqrt{2}}\mu_3 v_s}. \tag{7}$$

The mixing of the CP-even states h and s will yield two CP-even mass eigenstates h_1 and h_2 The mass of the pseudoscalar χ is, taking into account the extremum conditions,

$$m_\chi^2 = -\frac{9}{2\sqrt{2}}\mu_3 v_s, \tag{8}$$

which is proportional to μ_3 as it explicitly breaks the $U(1)$ symmetry.

We express the potential parameters in terms of physical quantities in the zero-temperature vacuum, that is the

masses m_1^2 and m_1^2 of real scalars, their mixing angle θ, pseudoscalar mass m_χ^2, and the VEVs v_h and v_s,

$$\lambda_H = \frac{m_1^2 + m_2^2 + (m_1^2 - m_2^2)\cos 2\theta}{4v_h^2}, \tag{9}$$

$$\lambda_S = \frac{3(m_1^2 + m_2^2) + 2m_\chi^2 + 3(m_2^2 - m_1^2)\cos 2\theta}{12v_s^2}, \tag{10}$$

$$\lambda_{SH} = \frac{(m_1^2 - m_2^2)\sin 2\theta}{2v_s v_h}, \tag{11}$$

$$\mu_H^2 = -\frac{1}{4}(m_1^2 + m_2^2) + \frac{1}{4v_h}(m_2^2 - m_1^2) \times (v_h \cos 2\theta + v_s \sin 2\theta), \tag{12}$$

$$\mu_S^2 = -\frac{1}{4}(m_1^2 + m_2^2) + \frac{1}{6}m_\chi^2 + \frac{1}{4v_s}(m_1^2 - m_2^2) \times (v_s \cos 2\theta - v_h \sin 2\theta), \tag{13}$$

$$\mu_3 = -\frac{2\sqrt{2}}{9}\frac{m_\chi^2}{v_s}. \tag{14}$$

Both the Higgs doublet and the singlet will get a VEV, with the Higgs VEV given by $v_h = v = 246.22$ GeV. We identify h_1 with the SM Higgs boson with mass $m_1 = 125.09$ GeV [80].

III. THEORETICAL AND EXPERIMENTAL CONSTRAINTS

We impose various theoretical and experimental constraints on the parameter space of the model.

First of all, the potential (1) is bounded from below if

$$\lambda_H > 0, \qquad \lambda_S > 0, \qquad \lambda_{SH} + 2\sqrt{\lambda_H \lambda_S} > 0. \tag{15}$$

Secondly, we require the couplings to be unitary and perturbative. The unitarity constraints in the $s \to \infty$ limit are given by

$$|\lambda_H| \leq 4\pi, \qquad |\lambda_S| \leq 4\pi, \qquad |\lambda_{SH}| \leq 8\pi, \tag{16}$$

$$|3\lambda_H + 2\lambda_S \pm \sqrt{9\lambda_H^2 - 12\lambda_H\lambda_S + 4\lambda_S^2 + 2\lambda_{SH}^2}| \leq 8\pi, \tag{17}$$

where the last condition, in the $\lambda_{SH} = 0$ limit, yields $|\lambda_H| \leq \frac{4}{3}\pi$ and $|\lambda_S| \leq 2\pi$. We also calculate unitarity constraints at finite energy with the help of the latest version [81] of the SARAH package [82–85]. Scattering at finite energy allows us to set a bound on the cubic coupling μ_3.

To ensure the validity of perturbation theory, loop corrections to couplings should be smaller than their tree-level values. The model is perturbative [86] if $|\lambda_H| \leq \frac{2}{3}\pi$, $|\lambda_S| \leq \pi$, and $|\lambda_{SH}| \leq 4\pi$.

We require that our $\mathcal{HS}$ vacuum be the global one: this implies that

$$m_\chi^2 < \frac{9m_1^2 m_2^2}{m_1^2 \cos^2\theta + m_2^2 \sin^2\theta}, \tag{18}$$

which for $\sin\theta \approx 0$ is approximated by $m_\chi \lesssim 3m_2$. This bound appears to be stronger than the constraint on the cubic coupling from unitarity at finite-energy scattering.

If the mass of $x \equiv \chi$ or h_2 is less than $m_h/2$, then the Higgs invisible decay width into this particle is given by

$$\Gamma_{h\to xx} = \frac{g_{hxx}}{8\pi}\sqrt{1 - 4\frac{m_x^2}{m_h^2}}, \tag{19}$$

with

$$g_{h1\chi\chi} = \frac{m_h^2 + m_\chi^2}{v_S}, \tag{20}$$

$$g_{h1h_2h_2} = \frac{1}{vv_S}\left[\left(\frac{1}{2}m_h^2 + m_2^2\right)(v\cos\theta + v_S\sin\theta) + \frac{1}{6}vm_\chi^2\cos\theta\right]\sin 2\theta. \tag{21}$$

The invisible Higgs branching ratio is then given by

$$\mathrm{BR}_{\mathrm{inv}} = \frac{\Gamma_{h\to\chi\chi} + \Gamma_{h\to h_2h_2}}{\Gamma_{h_1\to\mathrm{SM}} + \Gamma_{h\to\chi\chi} + \Gamma_{h\to h_2h_2}}, \tag{22}$$

which is constrained to be below about 0.24 at 95% confidence level [87,88] by direct measurements and below about 0.17 by statistical fits of all Higgs couplings [89,90] (decays of the resulting h_2 into the SM may be visible [16], but these points are already excluded by direct detection in any case). In extended Higgs models [91], the mixing phenomenology can be more complicated.

The mixing angle between h and s is constrained from the measurements of the Higgs couplings at the LHC to $|\sin\theta| \leq 0.5$ for $m_2 \lesssim m_h$ and $|\sin\theta| \leq 0.37$ for $m_2 \gtrsim m_h$; for the latter case, we have an ever stronger constraint from the mass of the W boson down to $|\sin\theta| \leq 0.2$ for larger values of m_2 [92].

Last, but not least, we require that the relic density of χ be equal to the value $\Omega_{\mathrm{DM}}h^2 = 0.120 \pm 0.001$ from recent Planck data [93].

IV. DIRECT DETECTION AND GRAVITATIONAL WAVE SIGNALS

For the scan of the parameter space, we choose m_χ, m_2, and $\sin\theta$ as the free parameters, while v_s is used to fit the DM

relic density. We generate the free parameter values in the following ranges: $m_\chi \in [25, 1000]$ GeV, $m_2 \in [25, 4000]$ GeV, and $\sin\theta \in [-0.5, 0.5]$. We use the micrOMEGAs package [94] to fit the DM relic density and CosmoTransitions [95] for the calculation of phase transitions and the Euclidean action to determine tunneling rates. The stochastic gravitational wave signals were calculated using the formulas of Ref. [96] for the nonrunaway case. At the temperature T_* at which gravitational waves are being produced, the spectrum is a function of the parameters,

$$\alpha = \frac{\rho_{\rm vac}}{\rho^*_{\rm rad}}, \tag{23}$$

where $\rho^*_{\rm rad} = g_* \pi^2 T_*^4/30$ and g_* is the number of relativistic degrees of freedom (d.o.f.) in the plasma at temperature T_*, and

$$\frac{\beta}{H_*} = T_* \frac{dS}{dT}\bigg|_{T_*}, \tag{24}$$

where S is the Euclidean action of a critical bubble.

The micrOMEGAs is also used to compute predictions for direct detection signals, to which we add the tiny loop correction. Unlike in the $\mathbb{Z}_2$ pseudo-Goldstone DM model, the tree-level direct detection DM amplitude contains a term that does not vanish at zero momentum transfer, so

$$\mathcal{A}_{\rm dd}(t \approx 0) \propto \lambda_{SH}\mu_3. \tag{25}$$

For a large part of the parameter space, however, this term is small enough, which allows one to explain the negative experimental results from DM direct detection experiments for a wide range of pseudo-Goldstone DM masses.

In the high temperature approximation (A8), the mass terms acquire thermal corrections,

$$\mu_H^2(T) = \mu_H^2 + c_H T^2, \qquad \mu_S^2(T) = \mu_H^2 + c_S T^2, \tag{26}$$

with the coefficients,

$$c_H = \frac{1}{48}(9g^2 + 3g'^2 + 12y_t^2 + 24\lambda_H + 4\lambda_{SH}), \tag{27}$$

$$c_S = \frac{1}{6}(2\lambda_S + \lambda_{SH}). \tag{28}$$

For numerical calculations of gravitational wave signals, the exact expression of the thermal potential is used.

We present in Fig. 1, the results of our scans for the direct detection signal. In the left panel, we present, for illustration, the behavior of spin-independent direct detection cross section $\sigma_{\rm SI}$ as a function of DM mass m_χ for fixed values of $m_2 = 300$ GeV and $\sin\theta = 0.05$. Red lines show the current limit from the XENON1T experiment [10] and the future bound from the projected XENONnT experiment [97]. While the usual $\mathbb{Z}_2$ scalar singlet DM is excluded below O(TeV) masses, except for the Higgs resonance region, the suppression of the pseudo-Goldstone cross section in this model allows for lighter DM candidates. The two pronounced dips in the cross section are given by the Higgs resonance at $m_h/2$ and the h_2 resonance at $m_2/2$.

The direct detection signal varies over a wide range and is proportional to μ_3^2. Because the amplitude is proportional to $\sin\theta\cos\theta$, larger mixing angles also produce larger direct detection signal. The right panel in Fig. 1 presents the results of the whole scan, coded in grey-scale by the mixing angle $|\sin\theta|$; empty points are excluded by the constraint on the Higgs invisible branching ratio. The points shown satisfy all other constraints with the exception of the collider constraints [92] on $|\sin\theta|$ (as seen, most such points are already excluded by direct detection). Note that the $\mathrm{BR}_{\rm inv}$ can exclude points with $m_\chi > m_h/2$, because the

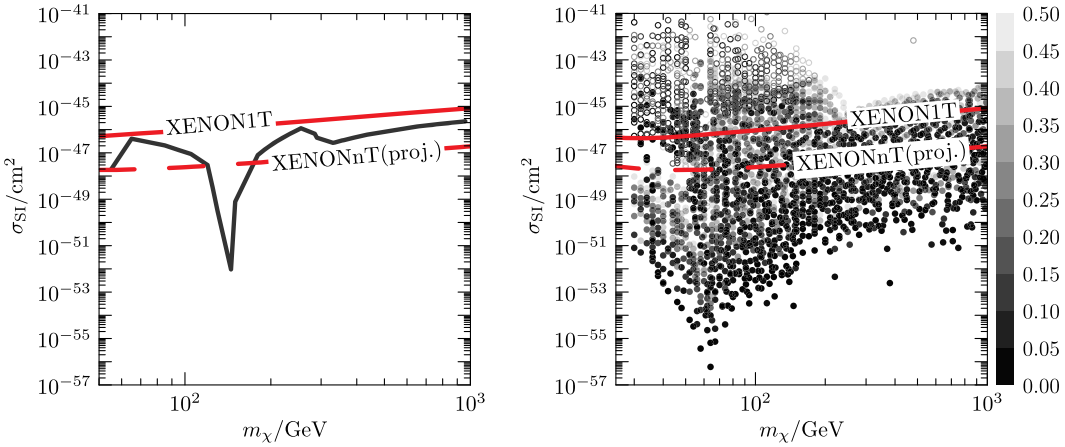

FIG. 1. Left panel: Spin-independent direct detection cross section $\sigma_{\rm SI}$ as a function of the DM mass m_χ for fixed $m_2 = 300$ GeV and $\sin\theta = 0.05$. The bound from the XENON1T experiment is shown in red and the predicted sensitivity of the XENONnT experiment in dashed red. Right panel: Scatter plot of the results in $(m_\chi, \sigma_{\rm SI})$ plane in the grey-scale representing the dependence on $|\sin\theta|$. The upper bound in $\sigma_{\rm SI}$ is given by the requirement that the (v_h, v_s) minimum be the global one. In unfilled points, the Higgs invisible width surpasses the experimental limit.

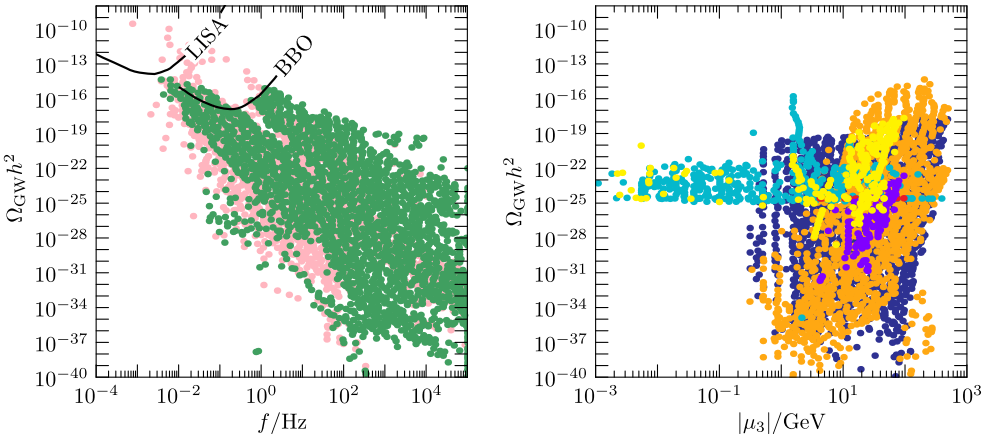

FIG. 2. Left panel: Scatter plot for the peak power of GWs vs the frequency together with the sensitivity curves of the LISA and BBO experiments. Light red points are forbidden and darker green points are allowed by the results of the XENON1T direct detection searches; both sets of points pass all other constraints, including the relic density. Right panel: The dependence of the peak power of GWs on the value of cubic coupling for the points that pass all constraints including direct detection. The color code shows the nature of the phase transition that gives the strongest signal: $\mathcal{O} \to \mathcal{S}$ in orange, $\mathcal{S} \to \mathcal{S}$ in dark blue, $\mathcal{S} \to \mathcal{HS}$ in cyan, $\mathcal{HS} \to \mathcal{HS}$ in yellow, $\mathcal{H} \to \mathcal{HS}$ in purple, $\mathcal{O} \to \mathcal{H}$ in red.

Higgs boson can decay invisibly also to two h_2 if it is light enough. Early kinetic decoupling [98,99] may additionally enhance $\mathrm{BR}_{\rm inv}$ several times [32], but, in practice, this would not change the parameter space of GW signals. In particular, all our points with a potentially measurable GW signal have $m_\chi, m_2 > m_h/2$. The upper bound on $\sigma_{\rm SI}$ arises from the requirement the $\mathcal{HS}$ vacuum be global, which bound is stronger than that from unitarity that also constrains the points from above.

In Fig. 2, we present the predicted stochastic GW signal together with the predicted sensitivity curves of the future LISA and the BBO satellite experiments. We used bubble wall velocity $v_{\rm w} = 0.5$ and the fraction $\kappa_{\rm turb} = 0.05\kappa_{\rm v}$ in a turbulent motion that is converted into gravitational waves following [96], where the fraction $\kappa_{\rm v}$ of vacuum energy converted into gravitational waves is given in [100]. To avoid cluttering the plot, we only show the peak power of each GW spectrum. In the left panel, light red points are excluded by the XENON1T direct detection constraints, while the darker green points are still allowed by direct detection; all points not satisfying the other constraints have been excluded. In the right panel, we depict the dependence of the GW signal on the cubic coupling μ_3. The color code shows the nature of the phase transition that yields the strongest signal in a sequence of phase transitions. The largest signal is produced by the $\mathcal{O} \to \mathcal{S}$ transitions, enhanced by a sizable cubic coupling. Because $m_\chi \propto \mu_3$, there is a similar dependence on m_χ/m_2. The strongest signals can be produced at roughly $m_\chi \approx 2.3 m_2$.

In the left panel of Fig. 3, we show the correlation between the gravitational wave signal and the direct detection cross section.

We have also calculated the signal-to-noise ratio for the BBO experiment, shown in the right panel of Fig. 3 with the same color code as Fig. 1. The horizontal thick line shows

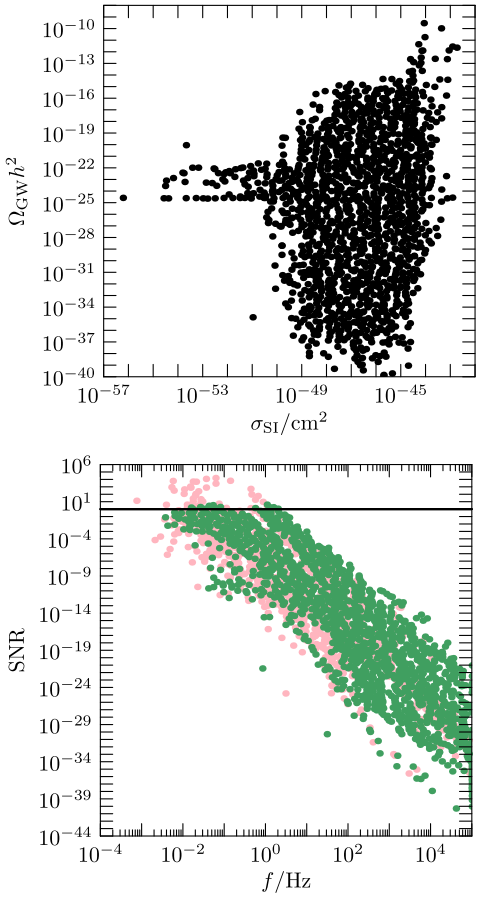

FIG. 3. Left panel: Scatter plot for the peak power of GWs vs direct detection cross section. The points pass all other constraints. Right panel: Signal-to-noise ratios of the data points for the BBO experiment. Light red points are forbidden and darker green points are allowed by the results of the XENON1T direct detection searches; both sets of points pass all other constraints. The horizontal thick line shows SNR = 1.

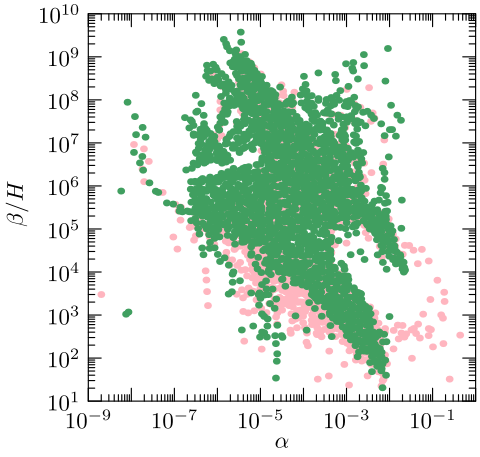

FIG. 4. β/H vs α. Light red points are forbidden and darker green points are allowed by the results of the XENON1T direct detection searches.

SNR $= 1$; the actual detection threshold is expected to be within an order of magnitude of it [96].

Because the direct detection cross section is proportional to μ_3^2, the points on the left panel of Fig. 2 with the highest GW signal are excluded. Note, however, that the direct detection signal can still be small even for a sizeable GW signal, because the Higgs portal λ_{SH} is on the order of (0.01). This is in contrast with $\lambda_{SH} \sim 1$ in Ref. [74] with the assumption that the $\mathbb{Z}_3$ symmetry is unbroken in our vacuum.

Figure 4 shows the range of β/H vs α with the same color code as Fig. 1. While Ref. [101] showed that for α close to unity the gravitational wave signal is suppressed, our values of α are quite smaller than one.

V. CONCLUSIONS

We have studied the $\mathbb{Z}_3$ complex scalar singlet DM model, where only the cubic coupling of the singlet explicitly breaks a global $U(1)$ symmetry. The model has two phases with stable DM. In the phase where the $\mathbb{Z}_3$ is spontaneously broken, the residual CP-like $\mathbb{Z}_2$ symmetry stabilizes the imaginary part of the complex singlet S as a pseudo-Goldstone DM candidate. The DM direct detection cross section can be considerably suppressed by the small momentum transfer or the resonance at half the mass of the heavy singletlike particle.

While we may be unable to discover the pseudo-Goldstone DM via direct detection, it may be testable by other means. In this model, a stochastic gravitational wave background can arise from the first-order phase transitions due to the presence of a cubic coupling for the singlet. The strongest signals, which can potentially be observed by the future BBO experiment, are produced in the $\mathcal{O} \to \mathcal{S}$ phase transition (if present) at $m_\chi \approx 2.3 m_2$. The strength of the gravitational wave signal is anticorrelated with a small mixing angle and is, therefore, greater where the direct detection cross section is smaller (at fixed cubic coupling).

ACKNOWLEDGMENTS

We would like to thank Matti Heikinheimo and Christian Gross for useful comments. This work was supported by the Estonian Research Council Grant No. PRG434, the Grant No. IUT23-6 of the Estonian Ministry of Education and Research, and by the European Union through the ERDF Centre of Excellence program Project No. TK133.

APPENDIX: THERMAL EFFECTIVE POTENTIAL

At the one-loop level, the quantum corrections to the scalar potential in the $\overline{\text{MS}}$ renormalization scheme are given by

$$\Delta V = \sum_i \frac{1}{64\pi^2} n_i m_i^4 \left(\ln \frac{m_i^2}{\mu^2} - c_i \right), \tag{A1}$$

where n_i are the d.o.f. of the ith field, m_i are field-dependent masses, and the constants $c_i = \frac{3}{2}$ for scalars and fermions and $c_i = \frac{5}{6}$ for vector bosons. The masses and d.o.f. n_i of the fields are given in Table I. The field-dependent masses of h and s are given by the eigenvalues $m_{1,2}^2$ of the mass matrix of the CP-even eigenstates with elements given by

$$(m_R^2)_{11} = \mu_H^2 + 3h^2\lambda_H + \frac{1}{2}\lambda_{SH} s^2, \tag{A2}$$

$$(m_R^2)_{12} = \lambda_{SH} h s, \tag{A3}$$

$$(m_R^2)_{22} = \mu_S^2 + 3\lambda_S s^2 + \frac{3}{2}\sqrt{2}\mu_3 s + \frac{1}{2} h^2 \lambda_{SH}. \tag{A4}$$

We neglect the contributions of the Goldstone bosons G^0 and $G^\pm$ as unimportant numerically. To calculate the effective potential in the case of negative field-dependent masses, we substitute $\ln m_i^2 \to \ln |m_i^2|$, which is equivalent to analytical continuation [102]. We set the renormalization scale to $\mu = M_t$.

We add a counterterm potential,

$$\delta V = \delta\mu_H^2 |H|^2 + \delta\lambda_H |H|^4 + \delta\mu_S^2 |S|^2 + \delta\lambda_S |S|^4 + \delta\lambda_{SH} |S|^2 |H|^2 + \frac{\delta\mu_3}{2}(S^3 + S^{\dagger 3}) + \delta V_0, \tag{A5}$$

TABLE I. Field-dependent masses and the numbers of d.o.f.

Field i	m_i^2	n_i
h	m_1^2	1
s	m_2^2	1
χ	$\mu_S^2 + \lambda_S s^2 - \frac{3}{\sqrt{2}}\mu_3 s + \frac{1}{2}\lambda_{SH} h^2$	1
Z^0	$\frac{1}{4}(g^2 + g'^2)h^2$	3
$W^\pm$	$\frac{1}{4} g^2 h^2$	6
t	$\frac{1}{2} y_t h^2$	-12

in order to fix the VEVs and the mass matrix in our $\mathcal{HS}$ minimum to their tree-level values.

The thermal corrections to the potential are given by

$$V_T = \frac{T^4}{2\pi^2}\sum_i n_i J_\mp\left(\frac{m_i}{T}\right), \tag{A6}$$

where

$$J_\mp = \pm\int_0^\infty dy y^2 \ln\left[1 \mp \exp\left(-\sqrt{y^2+x^2}\right)\right], \tag{A7}$$

with the $-$ sign applied to bosons and the $+$ sign to fermions. In the high-temperature limit $m/T \ll 1$, the thermal contributions are given by

$$V_T(T) = \frac{T^2}{24}\sum_i n_i m_i^2. \tag{A8}$$

The full thermally corrected effective potential is then

$$V^{(1)} = V + \Delta V + \delta V + V_T. \tag{A9}$$

The counterterm potential δV is chosen such as to keep quantum corrections to the masses, to mixing between h and s and to the VEVs zero. The counterterms are given by

$$\delta\lambda_H = \frac{1}{2v^3}(\partial_h\Delta V - v\partial_h^2\Delta V), \tag{A10}$$

$$\delta\lambda_S = \frac{1}{6v_S^3}(4\partial_s\Delta V - v_S\partial_\chi^2\Delta V - 3v_S\partial_s^2\Delta V), \tag{A11}$$

$$\delta\lambda_{SH} = -\frac{1}{vv_S}\partial_h\partial_s\Delta V, \tag{A12}$$

$$\delta\mu_H^2 = \frac{1}{2v}(-3\partial_h\Delta V + v_s\partial_h\partial_s\Delta V + v\partial_h^2\Delta V), \tag{A13}$$

$$\delta\mu_S^2 = -\frac{1}{6v_S}(v_S\partial_\chi^2\Delta V + 8\partial_s\Delta V - 3v_S\partial_s^2\Delta V - 3v\partial_h\partial_s\Delta V), \tag{A14}$$

$$\delta\mu_3 = \frac{2\sqrt{2}}{9v_S^2}(v_S\partial_\chi^2\Delta V - \partial_s\Delta V), \tag{A15}$$

where we take $h = v$, $s = v_S$, $\chi = 0$ after taking the derivatives.

[1] V. Silveira and A. Zee, Scalar phantoms, Phys. Lett. B **161**, 136 (1985).
[2] J. McDonald, Gauge singlet scalars as cold dark matter, Phys. Rev. D **50**, 3637 (1994).
[3] V. Barger, P. Langacker, M. McCaskey, M. Ramsey-Musolf, and G. Shaughnessy, Complex singlet extension of the Standard Model, Phys. Rev. D **79**, 015018 (2009).
[4] C. P. Burgess, M. Pospelov, and T. ter Veldhuis, The minimal model of nonbaryonic dark matter: A singlet scalar, Nucl. Phys. **B619**, 709 (2001).
[5] J. M. Cline, K. Kainulainen, P. Scott, and C. Weniger, Update on scalar singlet dark matter, Phys. Rev. D **88**, 055025 (2013); Erratum, Phys. Rev. D **92**, 039906 (2015).
[6] A. Djouadi, O. Lebedev, Y. Mambrini, and J. Quevillon, Implications of LHC searches for Higgs–portal dark matter, Phys. Lett. B **709**, 65 (2012).
[7] P. Athron *et al.*, Status of the scalar singlet dark matter model, Eur. Phys. J. C **77**, 568 (2017).
[8] G. Arcadi, A. Djouadi, and M. Raidal, Dark matter through the Higgs portal, arXiv:1903.03616.
[9] D. S. Akerib *et al.*, Results from a Search for Dark Matter in the Complete LUX Exposure, Phys. Rev. Lett. **118**, 021303 (2017).
[10] E. Aprile *et al.*, Dark Matter Search Results from a One Ton-Year Exposure of XENON1T, Phys. Rev. Lett. **121**, 111302 (2018).
[11] X. Cui *et al.*, Dark Matter Results from 54-Ton-Day Exposure of PandaX-II Experiment, Phys. Rev. Lett. **119**, 181302 (2017).
[12] C. Gross, O. Lebedev, and T. Toma, Cancellation Mechanism for Dark-Matter–Nucleon Interaction, Phys. Rev. Lett. **119**, 191801 (2017).
[13] C.-W. Chiang, M. J. Ramsey-Musolf, and E. Senaha, Standard Model with a complex scalar singlet: Cosmological implications and theoretical considerations, Phys. Rev. D **97**, 015005 (2018).
[14] D. Azevedo, M. Duch, B. Grzadkowski, D. Huang, M. Iglicki, and R. Santos, One-loop contribution to dark matter-nucleon scattering in the pseudoscalar dark matter model, J. High Energy Phys. 01 (2019) 138.
[15] K. Ishiwata and T. Toma, Probing pseudo Nambu-Goldstone boson dark matter at loop level, J. High Energy Phys. 12 (2018) 089.
[16] K. Huitu, N. Koivunen, O. Lebedev, S. Mondal, and T. Toma, Probing pseudo-Goldstone dark matter at the LHC, Phys. Rev. D **100**, 015009 (2019).
[17] T. Alanne, M. Heikinheimo, V. Keus, N. Koivunen, and K. Tuominen, Direct and indirect probes of Goldstone dark matter, Phys. Rev. D **99**, 075028 (2019).
[18] D. Azevedo, M. Duch, B. Grzadkowski, D. Huang, M. Iglicki, and R. Santos, Testing scalar versus vector dark matter, Phys. Rev. D **99**, 015017 (2019).
[19] J. M. Cline and T. Toma, Pseudo-Goldstone dark matter confronts cosmic ray and collider anomalies, Phys. Rev. D **100**, 035023 (2019).
[20] X.-M. Jiang, C. Cai, Z.-H. Yu, Y.-P. Zeng, and H.-H. Zhang, Pseudo-Nambu-Goldstone dark matter and two Higgs doublets, Phys. Rev. D **100**, 075011 (2019).

[21] M. Jiang, L. Bian, W. Huang, and J. Shu, Impact of a complex singlet: Electroweak baryogenesis and dark matter, Phys. Rev. D **93**, 065032 (2016).
[22] A. Alves, T. Ghosh, H.-K. Guo, and K. Sinha, Resonant di-Higgs production at gravitational wave benchmarks: A collider study using machine learning, J. High Energy Phys. 12 (2018) 070.
[23] A. Alves, T. Ghosh, H.-K. Guo, K. Sinha, and D. Vagie, Collider and gravitational wave complementarity in exploring the singlet extension of the Standard Model, J. High Energy Phys. 04 (2019) 052.
[24] E. Ma, Z(3) dark matter and two-loop neutrino mass, Phys. Lett. B **662**, 49 (2008).
[25] G. Belanger, K. Kannike, A. Pukhov, and M. Raidal, Z_3 scalar singlet dark matter, J. Cosmol. Astropart. Phys. 01 (2013) 022.
[26] G. Arcadi, F. S. Queiroz, and C. Siqueira, The semi-Hooperon: Gamma-ray and anti-proton excesses in the Galactic Center, Phys. Lett. B **775**, 196 (2017).
[27] Y. Cai and A. Spray, Low-temperature enhancement of semi-annihilation and the AMS-02 positron anomaly, J. High Energy Phys. 10 (2018) 075.
[28] Y. Hochberg, E. Kuflik, T. Volansky, and J. G. Wacker, Mechanism for Thermal Relic Dark Matter of Strongly Interacting Massive Particles, Phys. Rev. Lett. **113**, 171301 (2014).
[29] S.-M. Choi and H. M. Lee, SIMP dark matter with gauged Z_3 symmetry, J. High Energy Phys. 09 (2015) 063.
[30] N. Daci, I. De Bruyn, S. Lowette, M. H. G. Tytgat, and B. Zaldivar, Simplified SIMPs and the LHC, J. High Energy Phys. 11 (2015) 108.
[31] S.-M. Choi, Y.-J. Kang, and H. M. Lee, On thermal production of self-interacting dark matter, J. High Energy Phys. 12 (2016) 099.
[32] A. Hektor, A. Hryczuk, and K. Kannike, Improved bounds on $\mathbb{Z}_3$ singlet dark matter, J. High Energy Phys. 03 (2019) 204.
[33] P. Ko and Y. Tang, Galactic center γ-ray excess in hidden sector DM models with dark gauge symmetries: Local Z_3 symmetry as an example, J. Cosmol. Astropart. Phys. 01 (2015) 023.
[34] P. Ko and Y. Tang, Self-interacting scalar dark matter with local Z_3 symmetry, J. Cosmol. Astropart. Phys. 05 (2014) 047.
[35] J. Guo, Z. Kang, P. Ko, and Y. Orikasa, Accidental dark matter: Case in the scale invariant local B-L model, Phys. Rev. D **91**, 115017 (2015).
[36] N. Bernal, C. Garcia-Cely, and R. Rosenfeld, WIMP and SIMP dark matter from the spontaneous breaking of a Global group, J. Cosmol. Astropart. Phys. 04 (2015) 012.
[37] T. Hambye, Hidden vector dark matter, J. High Energy Phys. 01 (2009) 028.
[38] T. Hambye and M. H. Tytgat, Confined hidden vector dark matter, Phys. Lett. B **683**, 39 (2010).
[39] C. Arina, T. Hambye, A. Ibarra, and C. Weniger, Intense Gamma-ray lines from hidden vector dark matter decay, J. Cosmol. Astropart. Phys. 03 (2010) 024.
[40] F. D'Eramo and J. Thaler, Semi-annihilation of dark matter, J. High Energy Phys. 06 (2010) 109.
[41] G. Belanger, K. Kannike, A. Pukhov, and M. Raidal, Impact of semi-annihilations on dark matter phenomenology–An example of Z_N symmetric scalar dark matter, J. Cosmol. Astropart. Phys. 04 (2012) 010.
[42] G. Bélanger, K. Kannike, A. Pukhov, and M. Raidal, Minimal semi-annihilating $\mathbb{Z}_N$ scalar dark matter, J. Cosmol. Astropart. Phys. 06 (2014) 021.
[43] B. P. Abbott *et al.*, Observation of Gravitational Waves from a Binary Black Hole Merger, Phys. Rev. Lett. **116**, 061102 (2016).
[44] B. P. Abbott *et al.*, GW151226: Observation of Gravitational Waves from a 22-Solar-Mass Binary Black Hole Coalescence, Phys. Rev. Lett. **116**, 241103 (2016).
[45] C. J. Hogan, Nucleation of cosmological phase transitions, Phys. Lett. **133B**, 172 (1983).
[46] P. J. Steinhardt, Relativistic detonation waves and bubble growth in false vacuum decay, Phys. Rev. D **25**, 2074 (1982).
[47] E. Witten, Cosmic separation of phases, Phys. Rev. D **30**, 272 (1984).
[48] V. Corbin and N. J. Cornish, Detecting the cosmic gravitational wave background with the big bang observer, Classical Quantum Gravity **23**, 2435 (2006).
[49] P. A. Seoane *et al.*, The gravitational Universe, arXiv:1305.5720.
[50] K. Kajantie, M. Laine, K. Rummukainen, and M. E. Shaposhnikov, Is there a Hot Electroweak Phase Transition at m(H) Larger or Equal to m(W)?, Phys. Rev. Lett. **77**, 2887 (1996).
[51] Y. Aoki, F. Csikor, Z. Fodor, and A. Ukawa, The endpoint of the first order phase transition of the SU(2) gauge Higgs model on a four-dimensional isotropic lattice, Phys. Rev. D **60**, 013001 (1999).
[52] A. Mazumdar and G. White, Cosmic phase transitions: Their applications and experimental signatures, Rep. Prog. Phys. **82**, 076901 (2019).
[53] J. R. Espinosa, B. Gripaios, T. Konstandin, and F. Riva, Electroweak Baryogenesis in non-minimal composite Higgs models, J. Cosmol. Astropart. Phys. 01 (2012) 012.
[54] J. M. Cline and K. Kainulainen, Electroweak baryogenesis and dark matter from a singlet Higgs, J. Cosmol. Astropart. Phys. 01 (2013) 012.
[55] J. R. Espinosa, T. Konstandin, and F. Riva, Strong electroweak phase transitions in the Standard Model with a singlet, Nucl. Phys. **B854**, 592 (2012).
[56] T. Alanne, K. Tuominen, and V. Vaskonen, Strong phase transition, dark matter and vacuum stability from simple hidden sectors, Nucl. Phys. **B889**, 692 (2014).
[57] T. Alanne, K. Kainulainen, K. Tuominen, and V. Vaskonen, Baryogenesis in the two doublet and inert singlet extension of the Standard Model, J. Cosmol. Astropart. Phys. 08 (2016) 057.
[58] T. Tenkanen, K. Tuominen, and V. Vaskonen, A strong electroweak phase transition from the inflaton field, J. Cosmol. Astropart. Phys. 09 (2016) 037.
[59] R. Zhou, W. Cheng, X. Deng, L. Bian, and Y. Wu, Electroweak phase transition and Higgs phenomenology in the Georgi-Machacek model, J. High Energy Phys. 01 (2019) 216.

[60] W. Cheng and L. Bian, From inflation to cosmological electroweak phase transition with a complex scalar singlet, Phys. Rev. D **98**, 023524 (2018).
[61] M. Kakizaki, S. Kanemura, and T. Matsui, Gravitational waves as a probe of extended scalar sectors with the first order electroweak phase transition, Phys. Rev. D **92**, 115007 (2015).
[62] K. Hashino, M. Kakizaki, S. Kanemura, P. Ko, and T. Matsui, Gravitational waves and Higgs boson couplings for exploring first order phase transition in the model with a singlet scalar field, Phys. Lett. B **766**, 49 (2017).
[63] V. Vaskonen, Electroweak baryogenesis and gravitational waves from a real scalar singlet, Phys. Rev. D **95**, 123515 (2017).
[64] P. Huang, A. J. Long, and L.-T. Wang, Probing the electroweak phase transition with Higgs factories and gravitational waves, Phys. Rev. D **94**, 075008 (2016).
[65] M. Artymowski, M. Lewicki, and J. D. Wells, Gravitational wave and collider implications of electroweak baryogenesis aided by non-standard cosmology, J. High Energy Phys. 03 (2017) 066.
[66] A. Beniwal, M. Lewicki, J. D. Wells, M. White, and A. G. Williams, Gravitational wave, collider and dark matter signals from a scalar singlet electroweak baryogenesis, J. High Energy Phys. 08 (2017) 108.
[67] W. Chao, H.-K. Guo, and J. Shu, Gravitational wave signals of electroweak phase transition triggered by dark matter, J. Cosmol. Astropart. Phys. 09 (2017) 009.
[68] L. Bian, H.-K. Guo, and J. Shu, Gravitational waves, baryon asymmetry of the universe and electric dipole moment in the *CP*-violating NMSSM, Chin. Phys. C **42**, 093106 (2018).
[69] F. P. Huang, Z. Qian, and M. Zhang, Exploring dynamical *CP* violation induced baryogenesis by gravitational waves and colliders, Phys. Rev. D **98**, 015014 (2018).
[70] A. Beniwal, M. Lewicki, M. White, and A. G. Williams, Gravitational waves and electroweak baryogenesis in a global study of the extended scalar singlet model, J. High Energy Phys. 02 (2019) 183.
[71] D. Croon, V. Sanz, and G. White, Model discrimination in gravitational wave spectra from dark phase transitions, J. High Energy Phys. 08 (2018) 203.
[72] P. S. B. Dev, F. Ferrer, Y. Zhang, and Y. Zhang, Gravitational waves from first-order phase transition in a simple axion-like particle model, J. Cosmol. Astropart. Phys. 11 (2019) 006.
[73] K. Kannike and M. Raidal, Phase transitions and gravitational wave tests of Pseudo-Goldstone dark matter in the softly broken U(1) scalar singlet model, Phys. Rev. D **99**, 115010 (2019).
[74] Z. Kang, P. Ko, and T. Matsui, Strong first order EWPT & strong gravitational waves in Z_3-symmetric singlet scalar extension, J. High Energy Phys. 02 (2018) 115.
[75] Ya. B. Zeldovich, I. Yu. Kobzarev, and L. B. Okun, Cosmological consequences of the spontaneous breakdown of discrete symmetry, Zh. Eksp. Teor. Fiz. **67**, 3 (1974) [Sov. Phys. JETP **40**, 1 (1974)], https://www-public.slac.stanford.edu/sciDoc/docMeta.aspx?slacPubNumber=SLAC-TRANS-0165.
[76] T. W. B. Kibble, Some implications of a cosmological phase transition, Phys. Rep. **67**, 183 (1980).
[77] T. W. B. Kibble, Topology of cosmic domains and strings, J. Phys. A **9**, 1387 (1976).
[78] A. Friedland, H. Murayama, and M. Perelstein, Domain walls as dark energy, Phys. Rev. D **67**, 043519 (2003).
[79] S. A. Abel, S. Sarkar, and P. L. White, On the cosmological domain wall problem for the minimally extended supersymmetric standard model, Nucl. Phys. **B454**, 663 (1995).
[80] G. Aad *et al.*, Combined Measurement of the Higgs Boson Mass in pp Collisions at $\sqrt{s} = 7$ and 8 TeV with the ATLAS and CMS Experiments, Phys. Rev. Lett. **114**, 191803 (2015).
[81] M. D. Goodsell and F. Staub, Unitarity constraints on general scalar couplings with SARAH, Eur. Phys. J. C **78**, 649 (2018).
[82] F. Staub, From superpotential to model files for FeynArts and CalcHep/CompHep, Comput. Phys. Commun. **181**, 1077 (2010).
[83] F. Staub, Automatic calculation of supersymmetric renormalization group equations and self energies, Comput. Phys. Commun. **182**, 808 (2011).
[84] F. Staub, SARAH 3.2: Dirac Gauginos, UFO output, and more, Comput. Phys. Commun. **184**, 1792 (2013).
[85] F. Staub, SARAH 4: A tool for (not only SUSY) model builders, Comput. Phys. Commun. **185**, 1773 (2014).
[86] R. N. Lerner and J. McDonald, Gauge singlet scalar as inflaton and thermal relic dark matter, Phys. Rev. D **80**, 123507 (2009).
[87] V. Khachatryan *et al.*, Searches for invisible decays of the Higgs boson in pp collisions at $\sqrt{s} = 7, 8$, and 13 TeV, J. High Energy Phys. 02 (2017) 135.
[88] Combined measurements of Higgs boson production and decay using up to 80 fb^{-1} of proton–proton collision data at $\sqrt{s} = 13$ TeV collected with the ATLAS experiment, CERN Report No. Tech. Rep. ATLAS-CONF-2018-031, 2018, https://cds.cern.ch/record/2629412.
[89] P. P. Giardino, K. Kannike, I. Masina, M. Raidal, and A. Strumia, The universal Higgs fit, J. High Energy Phys. 05 (2014) 046.
[90] G. Belanger, B. Dumont, U. Ellwanger, J. F. Gunion, and S. Kraml, Global fit to Higgs signal strengths and couplings and implications for extended Higgs sectors, Phys. Rev. D **88**, 075008 (2013).
[91] M. Raidal and A. Strumia, Hints for a non-standard Higgs boson from the LHC, Phys. Rev. D **84**, 077701 (2011).
[92] A. Ilnicka, T. Robens, and T. Stefaniak, Constraining extended scalar sectors at the LHC and beyond, Mod. Phys. Lett. A **33**, 1830007 (2018).
[93] N. Aghanim *et al.*, Planck 2018 results. VI. Cosmological parameters, arXiv:1807.06209.
[94] G. Bélanger, F. Boudjema, A. Goudelis, A. Pukhov, and B. Zaldivar, micrOMEGAs5.0: Freeze-in, Comput. Phys. Commun. **231**, 173 (2018).
[95] C. L. Wainwright, CosmoTransitions: Computing cosmological phase transition temperatures and bubble profiles with multiple fields, Comput. Phys. Commun. **183**, 2006 (2012).

[96] C. Caprini *et al.*, Science with the space-based interferometer eLISA. II: Gravitational waves from cosmological phase transitions, J. Cosmol. Astropart. Phys. 04 (2016) 001.
[97] K. Ni (XENON collaboration), The XENONnT dark matter experiment, DPF 2017, Fermilab, 2017.
[98] T. Binder, T. Bringmann, M. Gustafsson, and A. Hryczuk, Early kinetic decoupling of dark matter: when the standard way of calculating the thermal relic density fails, Phys. Rev. D **96**, 115010 (2017).
[99] M. Duch and B. Grzadkowski, Resonance enhancement of dark matter interactions: The case for early kinetic decoupling and velocity dependent resonance width, J. High Energy Phys. 09 (2017) 159.
[100] J. R. Espinosa, T. Konstandin, J. M. No, and G. Servant, Energy budget of cosmological first-order phase transitions, J. Cosmol. Astropart. Phys. 06 (2010) 028.
[101] D. Cutting, M. Hindmarsh, and D. J. Weir, Vorticity, kinetic energy, and suppressed gravitational wave production in strong first order phase transitions, arXiv:1906.00480.
[102] M. Bobrowski, G. Chalons, W. G. Hollik, and U. Nierste, Vacuum stability of the effective Higgs potential in the minimal supersymmetric Standard Model, Phys. Rev. D **90**, 035025 (2014); Erratum, Phys. Rev. D **92**, 059901 (2015).